

HYSTERESIS IN A ROTATING DIFFERENTIALLY HEATED SPHERICAL SHELL OF BOUSSINESQ FLUID *

GREGORY M. LEWIS[†] AND WILLIAM F. LANGFORD[‡]

Abstract. A mathematical model of convection of a Boussinesq fluid in a rotating spherical shell is analyzed using numerical computations guided by bifurcation theory. The fluid is differentially heated on its inner spherical surface, with the temperature increasing from both poles to a maximum at the equator. The model is assumed to be both rotationally symmetric about the polar axis and reflectionally symmetric across the equator. This work is an extension to spherical geometry of previous work on the differentially heated rotating annulus. The spherical geometry is motivated by applications to planetary atmospheres. As the temperature gradient increases from zero, large Hadley cells extending from equator to poles form immediately. For larger temperature differences, two or three convection cells appear in each hemisphere. An organizing centre is shown to exist, at which two saddle-node bifurcations come together in a codimension-2 hysteresis bifurcation (or cusp) point, providing a mechanism for hysteretic transitions between different cell patterns as the temperature gradient is varied.

Key words. cusp point, hysteresis bifurcation, flow transitions, Boussinesq fluid, flow in a rotating spherical shell, numerical computation, large-scale geophysical flow

AMS subject classifications. 37N10, 76U05, 37M99

1. Introduction. The atmosphere of a planet may be idealized as a spherical shell of fluid surrounding the spherical surface of the planet. Many factors affect the circulation of the atmosphere; chief among these are the rotation of the planet, the differential heating of the surface and atmosphere by the planet's sun, and the thickness and composition of the atmosphere itself. In this paper we construct an idealized mathematical model of such a planet, ignoring all local variations of surface features such as oceans, continents, mountains and glaciers. The symmetries of this model are exploited to make the computations more tractable.

On the inner boundary surface a temperature profile is prescribed to reflect the differential heating of the atmosphere by the sun, as follows. The average annual flux of solar radiation on a planet whose axis of rotation is tilted approximately 20° with respect to the plane that is perpendicular to the solar rays is nearly proportional to $-\cos(2\theta)$, see [19], where θ is the polar angle, which only differs from the latitude in its range (in particular the latitude is given by $\pi/2 - \theta$). This flux is independent of the azimuthal variable φ and is a maximum at the equator ($\theta = \pi/2$), and a minimum at the poles ($\theta = 0, \pi$). This profile is similar to the annual average of solar flux for many of the planets in our solar system, including Earth. Therefore, we choose the temperature on the inner boundary surface to be fixed at $T = T_r - \Delta T \cos(2\theta)$, where T_r is a reference temperature and the difference in the temperature from equator to pole is $2\Delta T$. On a real planet, a flux of radiation of this form would not result exactly in this prescribed temperature distribution on the surface, but we expect it to capture the gross effects of the differential heating. In the model, the spherical shell is filled with a Boussinesq fluid, which means that its density varies linearly with temperature.

* This work was supported in part by the Natural Sciences and Engineering Research Council of Canada and by the Fields Institute for Research in Mathematical Sciences.

[†] Faculty of Science, University of Ontario Institute of Technology, 2000 Simcoe Street North, Oshawa ON L1H 7K4, Canada (greg.lewis@uoit.ca)

[‡] Department of Mathematics and Statistics, University of Guelph, 50 Stone Road East, Guelph ON N1G 2W1, Canada (wlangfor@uoguelph.ca)

Thus, the gravitational force acting radially inward drives convective motions of the fluid when $\Delta T > 0$.

We assume that both the inner and outer spheres are rigid, and that the fluid satisfies no-slip conditions on both boundaries. For the temperature at the outer sphere, we assume insulating boundary conditions. Inside the spherical shell, the fluid satisfies the Navier-Stokes equations in the Boussinesq approximation. Complete details of the model are given in Section 2. The nonlinear equations for a steady state are solved using Newton iteration with Keller continuation from the trivial solution at $\Delta T = 0$. The linear stability problem is solved using the implicitly restarted Arnoldi method following a generalized Cayley transformation. The full methodology for analysis of the model is described in Sections 3 and 4 and the results are presented in Sections 5 and 6.

It is not possible in an Earth-bound laboratory to perform an experimental study of convection in a spherical shell as described here, because the gravitational force can not be directed radially towards the common center of the spheres. (However, experiments to study spherical convection with a central force field under weightless conditions in a space lab are an interesting possibility, see for example [11, 3].) Many laboratory experiments have been performed on a differentially heated rotating cylindrical annulus, with the Earth's gravity acting downward parallel to the cylinder axis and centrifugal force acting radially. These experiments typically used water as the working fluid. Much has been learned about the dynamics of large scale geophysical fluids from these laboratory experiments, even though the Reynolds number is significantly smaller in the experimental fluids than in actual geophysical flows [12, 24]. The Boussinesq approximation has been used as a basis for a mathematical model of the differentially heated rotating annulus, using laboratory-scale parameters and with water as the fluid [13, 20, 21]. The model has provided good agreement with the corresponding laboratory experiments.

Therefore, in this prototype mathematical model of a differentially heated rotating spherical shell of fluid, we adopt a philosophy of choosing the parameters of the fluid to be those of water and using the laboratory scale rather than the geophysical. In this way, the computations are tractable and the results obtained can be compared to both experiments and theoretical calculations for the better understood case of a differentially heated rotating annulus. This may provide insight into the how the geometry of the system leads to the observed flow transitions, and may serve as a step towards understanding the dynamical structure of planetary systems. Although we have made quantitative choices for the fluid and the boundary conditions, we expect that these choices will have little effect on qualitative features of the results. This is supported by the numerous studies that have been performed on the differentially heated rotating annulus. Many experiments have been performed with different forms of heating, different geometries of the apparatus and with different fluid properties, and it is found that these have little qualitative effect on the types of transitions and form of the transition curves that are observed.

The goal of this paper is to determine the flow patterns, their stabilities and their transitions (bifurcations) for a differentially heated rotating spherical shell, consistent with our modeling assumptions. There are three bifurcation parameters of interest: the temperature difference ΔT , the shell gap width R and the rotation rate Ω . The results presented in Section 5 show that the qualitative features of the flow patterns do not change for moderate changes of Ω , although the stability with respect to non-rotationally symmetric perturbations is affected. However, for even very small

$\Delta T > 0$, the fluid immediately begins to flow in a large stable convection cell with easterly flow toward the equator near the inner surface. This flow is similar to the Hadley cell, which exists in the atmosphere between approximately the equator and 30° latitude (in each hemisphere), except that it extends from equator to pole. In this paper, we refer to this convection cell as the Hadley cell. For larger values of ΔT , two or even three convection cells may appear between the equator and pole. The Hadley cell shrinks, always keeping one edge at the equator, while the additional cells appear between it and the pole. When a second cell exists next to the Hadley cell, it is characterized by a weaker counter-rotating flow, with a westerly component. The third cell, when it exists, has the same sense of rotation as the Hadley cell but lies near the pole. In every case, there is a region of high velocity azimuthal flow at high altitudes and mid-latitudes, resembling the Earth's *jet stream*.

Furthermore, we show that there exists a critical value of the pair $(R, \Delta T)$ that is a *hysteresis bifurcation point* (also called a *cusp point*), see Figure 1.1. This is a codimension-2 steady-state bifurcation that is well understood in mathematical bifurcation theory. The existence of this hysteresis point is demonstrated by an explicit calculation of its defining conditions in Section 6, where the study of this hysteresis bifurcation is presented in detail. Only its main features are outlined here. Figure 1.1 represents a generic hysteresis bifurcation. Here M is a manifold of steady states, existing for given parameters $(R, \Delta T)$, and the vertical axis represents the amplitude of a steady state (determined by the stream function in Section 6). In a neighborhood of a hysteresis bifurcation point, the number of steady states (on M) can vary from one to three as the parameters $(R, \Delta T)$ vary. When three steady states coexist in Figure 1.1, the middle one is unstable, but all other steady states not on the fold lines in Figure 1.1 remain stable (attracting). Furthermore, there are abrupt upward and downward transitions at two *fold bifurcations* (also called limit points or saddle-node bifurcations) as shown in Figure 1.1, that occur at both ends of an interval of the bifurcation parameter ΔT , for appropriate fixed R . If ΔT is varied back and forth through this interval, the system traces a *hysteresis loop* as shown in Figure 1.1. Between these two abrupt transitions there is an interval of ΔT that exhibits *bistability*; that is, two solutions are stable simultaneously.

1.1. Relationship to previous work. The fundamental problem of convection in spherical shells was formulated by Chandrasekhar [4, Ch. 6], who also solved the stability problem in the Boussinesq approximation for the spherically symmetric case, in terms of spherical harmonics. There is a large literature on spherically symmetric convection that is motivated by the Earth's core and mantle, where the boundary conditions have full spherical symmetry (in particular a constant temperature on the inner sphere), see for example [3, 5, 22, 32]. The present work differs from all of these because of the latitudinal temperature gradient.

Motivation for the present work is provided also by the classical Taylor-Couette experiment, in which the flow of a fluid (usually water) between two differentially rotating long coaxial cylinders is studied, see for example [2, 6, 9, 17]. In that experiment many interesting flow patterns may form, including *Taylor vortices*, which are invariant tori stacked coaxially between the cylinders in pairs with alternating clockwise and counterclockwise helical flows. There is no differential heating in the Taylor-Couette experiment; even so, the Taylor vortices resemble Hadley cells. Marcus and Tuckerman [25, 26] performed numerical simulations of the flow between two differentially rotating spheres (without heating) and found bifurcations to different numbers of cells that they called Taylor vortices, thus showing that Hadley-like cells

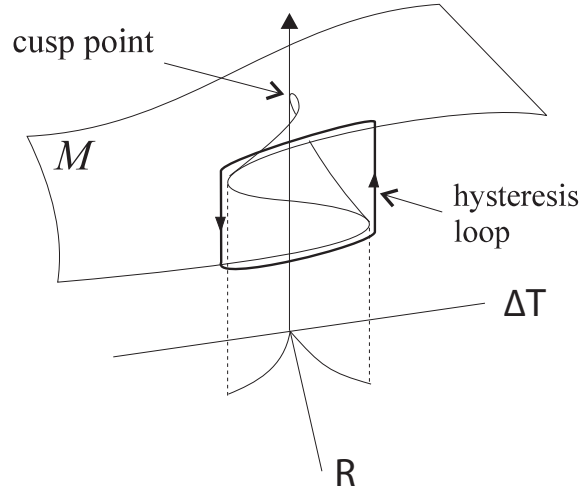


FIG. 1.1. The codimension 2 hysteresis bifurcation, showing the hysteresis loop as ΔT varies back and forth. The cusp shown in the $(R, \Delta T)$ parameter plane is the projection of the two curves of fold bifurcations onto this plane.

may form even without differential heating, if the spheres are rotated differentially. See also [14].

2. Model equations. We use the Navier-Stokes equations in the Boussinesq approximation to model the fluid flow within the spherical shell. In the Boussinesq approximation, the variations of all fluid properties, except the density, are considered to be negligible and the equation of state of the fluid is assumed to be

$$\rho = \rho_0 (1 - \alpha (T - T_r)), \quad (2.1)$$

where ρ is the density of the fluid, T is the temperature, α is the (constant) coefficient of thermal expansion, and ρ_0 is the density at a reference temperature T_r . The dimensionless quantity $\alpha (T - T_r)$ is assumed to be small. In the Boussinesq approximation the fluid is considered to be incompressible, which is a significant simplification.

The fluid is contained within a spherical shell with inner sphere of radius r_a and outer sphere of radius r_b . We assume gravity acts everywhere in the radial direction. The spherical shell rotates at rate Ω about the polar axis, and the inner and outer spheres rotate at the same rate. The equations are written in spherical polar coordinates in a frame of reference co-rotating at rate Ω with the shell. The radial, polar, and azimuthal coordinates are denoted r , θ , and φ , respectively, with unit vectors \mathbf{e}_r , \mathbf{e}_θ and \mathbf{e}_φ .

The Navier-Stokes Boussinesq equations describing the evolution of the vector fluid velocity, $\mathbf{u} = \mathbf{u}(r, \theta, \varphi, t) = w\mathbf{e}_r + v\mathbf{e}_\theta + u\mathbf{e}_\varphi$ and the temperature of the fluid, $T = T(r, \theta, \varphi, t)$ are:

$$\frac{\partial \mathbf{u}}{\partial t} = \nu \nabla^2 \mathbf{u} - 2\boldsymbol{\Omega} \times \mathbf{u} + [g\mathbf{e}_r + \boldsymbol{\Omega} \times (\boldsymbol{\Omega} \times \mathbf{r})] \alpha (T - T_r) - \frac{1}{\rho_0} \nabla p - (\mathbf{u} \cdot \nabla) \mathbf{u}, \quad (2.2)$$

$$\frac{\partial T}{\partial t} = \kappa \nabla^2 T - (\mathbf{u} \cdot \nabla) T, \quad (2.3)$$

$$\nabla \cdot \mathbf{u} = 0, \quad (2.4)$$

where $\mathbf{\Omega} = \Omega (\cos \theta \mathbf{e}_r - \sin \theta \mathbf{e}_\theta)$ is the rotation vector, $\Omega = |\mathbf{\Omega}|$ is the rate of rotation about the polar axis, p is the pressure deviation from $p_0 = \rho_0 g(R-r) + \rho_0 \Omega^2 r^2 \sin^2 \theta / 2$, $\mathbf{r} = r \mathbf{e}_r + \theta \mathbf{e}_\theta + \varphi \mathbf{e}_\varphi$, ν is the kinematic viscosity, κ is the coefficient of thermal diffusivity, g is the gravitational acceleration, ∇ is the usual gradient operator in spherical coordinates, u is the azimuthal fluid velocity, often referred to as the zonal velocity, v is the polar fluid velocity, and w is the radial fluid velocity. The spatial domain is defined by $r_a < r < r_b$, $0 \leq \varphi < 2\pi$, and $0 < \theta < \pi$. Thus, $\theta = 0, \pi$ correspond to the north and south poles of the shell respectively, while $\theta = \pi/2$ corresponds to the equator. The equations can be rewritten in planetary coordinates by performing the change of variable $\theta \rightarrow \pi/2 - \theta$. The values of ν and κ are chosen to be those of the fluid at the reference temperature T_r , and it is assumed that the difference between the temperature of the fluid and T_r is everywhere small enough so that ν and κ can be considered as constants. We have included the effects of centrifugal buoyancy in the equations via the term $\mathbf{\Omega} \times (\mathbf{\Omega} \times \mathbf{r})$. All dimensional quantities are measured in CGS units.

As described in the Introduction, the boundary conditions are

$$\begin{aligned} \mathbf{u} = 0, \quad T = T_r - \Delta T \cos(2\theta) & \quad \text{on } r = r_a, \\ \mathbf{u} = 0, \quad \frac{\partial T}{\partial r} = 0 & \quad \text{on } r = r_b, \end{aligned} \quad (2.5)$$

with 2π -periodicity in the azimuthal variable φ .

In this paper we investigate flows that preserve the symmetries of the model, that is, flows that are invariant under rotation about the polar axis (i.e. axisymmetric flows) and that are invariant under reflection across the equator (i.e. across the line defined by $\theta = \pi/2$). Therefore, we study solutions of (2.2) – (2.5) in the form

$$\begin{aligned} u = u(r, \theta, t) = u(r, \pi - \theta, t), \quad v = v(r, \theta, t) = v(r, \pi - \theta, t), \\ w = w(r, \theta, t) = w(r, \pi - \theta, t), \quad T = T(r, \theta, t) = T(r, \pi - \theta, t), \end{aligned} \quad (2.6)$$

The assumed symmetries significantly simplify the analysis. We may use the analysis of the symmetric system as a starting point for an analysis of the full system. Although it is not written explicitly, the solutions also depend on the parameters.

If we scale the radial coordinate as

$$r \rightarrow Rr', \quad (2.7)$$

where $R = r_b - r_a$ is the gap width, write the temperature as

$$T \rightarrow T' + T_r - \Delta T \cos(2\pi), \quad (2.8)$$

substitute these into (2.2) – (2.4), and drop the primes, we obtain the following axisymmetric equations describing the evolution of the fluid velocity $\mathbf{u} = w(r, \theta, t)\mathbf{e}_r + v(r, \theta, t)\mathbf{e}_\theta + u(r, \theta, t)\mathbf{e}_\varphi$, pressure deviation $p = p(r, \theta, t)$ and temperature deviation

$T = T(r, \theta, t)$:

$$\begin{aligned} \frac{\partial u}{\partial t} &= \nu_s \nabla_0^2 u - \nu_s \frac{1}{r^2 \sin^2 \theta} u - 2\Omega (\sin \theta w + \cos \theta v) \\ &\quad - \frac{1}{R} \left[(\mathbf{u} \cdot \nabla_0) u + \frac{\cos \theta}{r \sin \theta} uv + \frac{uw}{r} \right], \end{aligned} \quad (2.9)$$

$$\begin{aligned} \frac{\partial v}{\partial t} &= \nu_s \nabla_0^2 v - \nu_s \left(\frac{1}{r^2 \sin^2 \theta} v - \frac{2}{r^2} \frac{\partial w}{\partial \theta} \right) + 2\Omega \cos \theta u - \frac{1}{\rho_0 R r} \frac{\partial p}{\partial \theta} \\ &\quad - (\alpha \Omega^2 R r \sin \theta \cos \theta) (T - \Delta T \cos 2\theta) - \frac{1}{R} \left[(\mathbf{u} \cdot \nabla_0) v - \frac{\cos \theta}{r \sin \theta} u^2 + \frac{vw}{r} \right], \end{aligned} \quad (2.10)$$

$$\begin{aligned} \frac{\partial w}{\partial t} &= \nu_s \nabla_0^2 w - \nu_s \left(\frac{2 \cos \theta}{r^2 \sin \theta} v + \frac{2}{r^2} \frac{\partial v}{\partial \theta} + \frac{2}{r^2} w \right) + 2\Omega \sin \theta u - \frac{1}{\rho_0 R r} \frac{\partial p}{\partial r} \\ &\quad - \alpha (\Omega^2 R r \sin^2 \theta + g) (T - \Delta T \cos 2\theta) - \frac{1}{R} \left[(\mathbf{u} \cdot \nabla_0) w - \frac{1}{r} (u^2 + v^2) \right], \end{aligned} \quad (2.11)$$

$$\frac{\partial T}{\partial t} = \kappa_s \nabla_0^2 T + \frac{4\Delta T \kappa_s}{r^2} (\cos 2\theta + \cos^2 \theta) + \frac{2\Delta T}{R r} \sin 2\theta v - \frac{1}{R} (\mathbf{u} \cdot \nabla_0) T, \quad (2.12)$$

$$\nabla_0 \cdot \mathbf{u} = \frac{\partial w}{\partial r} + \frac{2}{r} w + \frac{1}{r} \frac{\partial v}{\partial \theta} + \frac{\cos \theta}{r \sin \theta} v = 0, \quad (2.13)$$

where $\nu_s = \nu/R^2$, $\kappa_s = \kappa/R^2$,

$$\nabla_0^2 = \frac{\partial^2}{\partial r^2} + \frac{2}{r} \frac{\partial}{\partial r} + \frac{1}{r^2} \frac{\partial^2}{\partial \theta^2} + \frac{\cos \theta}{r^2 \sin \theta} \frac{\partial}{\partial \theta},$$

$$\nabla_0 = \mathbf{e}_r \frac{\partial}{\partial r} + \mathbf{e}_\theta \frac{1}{r} \frac{\partial}{\partial \theta},$$

and

$$(\mathbf{u} \cdot \nabla_0) f = w \frac{\partial f}{\partial r} + \frac{v}{r} \frac{\partial f}{\partial \theta}, \quad (2.14)$$

for any scalar function $f = f(r, \theta, t)$. The domain is now expressed as $r_a/R < r < r_b/R$, $0 \leq \theta < \pi/2$, and the boundary conditions become

$$\begin{aligned} \mathbf{u} &= 0, & T &= 0 & \text{on } r &= \frac{r_a}{R}, \\ \mathbf{u} &= 0, & \frac{\partial T}{\partial r} &= 0 & \text{on } r &= \frac{r_b}{R}. \end{aligned} \quad (2.15)$$

The symmetry assumptions not only reduce the domain size, i.e. we now have $0 \leq \theta \leq \pi/2$, but they also effectively introduce new boundary conditions at the equator and the pole. In order to satisfy the symmetries, there can be no flow of fluid or heat across the equator or the pole. In addition, the condition $u = 0$ at the pole is necessary to ensure that no discontinuity occurs in the fluid velocity at the pole. Thus, we have the additional boundary conditions:

$$\begin{aligned} u, v &= 0, & \frac{\partial w}{\partial \theta} &= 0, & \frac{\partial T}{\partial \theta} &= 0 & \text{on } \theta &= 0, \\ v &= 0, & \frac{\partial u}{\partial \theta} &= \frac{\partial w}{\partial \theta} = 0, & \frac{\partial T}{\partial \theta} &= 0 & \text{on } \theta &= \pi/2. \end{aligned} \quad (2.16)$$

It is possible to write the equations completely in terms of dimensionless variables. However, this would not simplify the analysis, so we choose to work with the equations in the form (2.9) – (2.13). This follows previous numerical work on similar problems, e.g. [13, 31, 20].

3. Analysis.

3.1. Nonlinear equations for steady solution. The analysis begins with the computation of steady axisymmetric solutions that are invariant with respect to reflection across the equator; that is, we seek solutions of (2.9) – (2.13) that satisfy the boundary conditions (2.15) – (2.16) and are independent of time.

The method of stream functions is used to solve the steady equations. If v and w are written in terms of a (Stokes) stream function ξ , defined by

$$v = -\frac{1}{r \sin \theta} \frac{\partial \xi}{\partial r}, \quad w = \frac{1}{r^2 \sin \theta} \frac{\partial \xi}{\partial \theta}, \quad (3.1)$$

then the incompressibility condition (2.13) is automatically satisfied [1]. After using (3.1) to replace v and w in the equations, the pressure terms can be eliminated. Subsequently, the steady solution can be found from the resulting three equations in the three unknown functions u , ξ and T . These equations are found using the Maple symbolic computation software package, and are sufficiently complicated that no insight is gained by explicitly writing them here. The boundary conditions for u and T are given by (2.15) – (2.16) as before, while the conditions on v and w will be satisfied if ξ satisfies the boundary conditions

$$\begin{aligned} \xi = 0, \quad \frac{\partial \xi}{\partial \theta} = 0, \quad \frac{\partial^3 \xi}{\partial \theta^3} = 0 & \quad \text{on } \theta = 0 \\ \xi = 0, \quad \frac{\partial^2 \xi}{\partial \theta^2} = 0 & \quad \text{on } \theta = \frac{\pi}{2} \\ \xi = 0, \quad \frac{\partial \xi}{\partial r} = 0 & \quad \text{on } r = \frac{r_a}{R}, \frac{r_b}{R}. \end{aligned} \quad (3.2)$$

The numerical algorithm to solve this system of nonlinear equations is described in Section 4 and the steady axisymmetric solutions obtained are presented in Section 5.

3.2. Linear stability analysis. The linear stability of a steady solution is defined in terms of the eigenvalues of the linearization of the dynamical equations about that solution. If the real parts of *all* the eigenvalues are negative, then all perturbations from the steady solution will decay in the linearized equations. In this case, the solution is said to be linearly stable. If any of the eigenvalues has positive real part, then some small perturbations will grow, and the solution is linearly unstable. If there exist only eigenvalues with zero real part and negative real part, the solution is called neutrally stable. If the real part of an eigenvalue crosses the imaginary axis as a parameter is varied, then a qualitative change in the solution occurs; i.e., a bifurcation takes place. Flows corresponding to linearly stable steady solutions can be observed physically if the noise that is naturally present is sufficiently small. If a steady solution is linearly unstable, then the corresponding flow can not be observed because some small perturbations due to the noise will tend to grow. Thus, it is expected that bifurcations correspond to transitions in the observed flow.

We compute the steady axisymmetric solution and its linear stability as the parameters of the system change, and seek locations in the space of parameters where an eigenvalue crosses the imaginary axis. We are primarily interested in solutions

that do not break the assumed symmetry, and therefore, we initially require that this eigenvalue be associated with an eigenfunction that respects the symmetry.

If we write

$$u = u' + u_0, \quad \xi = \xi' + \xi_0, \quad T = T' + T_0, \quad (3.3)$$

where u_0, ξ_0, T_0 is a steady solution, and substitute into the three equations for $u, \xi,$ and T , we obtain the perturbation equations in $u', \xi',$ and T' . The trivial solution satisfies the perturbation equations, and it corresponds to u_0, ξ_0, T_0 . If the perturbation equations are linearized and we assume that the unknown functions may be written as

$$u'(r, \theta, t) = e^{\lambda t} \psi_u(r, \theta), \quad \xi'(r, \theta, t) = e^{\lambda t} \psi_\xi(r, \theta), \quad T'(r, \theta, t) = e^{\lambda t} \psi_T(r, \theta), \quad (3.4)$$

then a linear eigenvalue problem is obtained. Consequently, the eigenvalues λ can be found from the generalized eigenvalue problem of the form

$$\lambda \mathbf{A}_0 \Psi = \mathbf{L}_0 \Psi, \quad (3.5)$$

where

$$\Psi = \begin{pmatrix} \psi_u \\ \psi_\xi \\ \psi_T \end{pmatrix}$$

is the eigenfunction, and \mathbf{A}_0 and \mathbf{L}_0 are 3×3 matrices of linear differential operators.

The perturbations $u', \xi',$ and T' correspond to axisymmetric perturbations. If all eigenvalues corresponding to these perturbations have negative real part, then the steady solution u_0, ξ_0, T_0 is a linearly stable solution of the axisymmetric equations (2.9) – (2.13). For this steady solution to be a corresponding linearly stable solution of the full three-dimensional model (2.2) – (2.4), we must also compute the eigenvalues corresponding to the non-axisymmetric perturbations. To do this, we linearize the perturbation equations corresponding to the three-dimensional model, and we assume that the eigenfunctions have the form

$$\Phi(r, \theta, \varphi) = \hat{\Phi}_m(r, \theta) e^{im\varphi},$$

where $m = 1, 2, \dots$ is the azimuthal wave number. Unlike in the axisymmetric case, it is not possible to solve this problem using a stream function approach. However, due to the form of the eigenfunctions, it is possible to use the incompressibility condition and the equation for the azimuthal velocity to eliminate the pressure and the azimuthal velocity, resulting in a generalized eigenvalue problem for each wave number m . The eigenvalue problem has the form (3.5) with $\hat{\Psi}_m$ replacing Ψ , and where

$$\hat{\Psi}_m = \begin{pmatrix} \hat{v}_m \\ \hat{w}_m \\ \hat{T}_m \end{pmatrix},$$

and the functions $\hat{v}_m, \hat{w}_m, \hat{T}_m$ depend only on r and θ .

To ensure the continuity of solutions, we require that, for $m \neq 1$, $\hat{v}_m, \hat{w}_m, \hat{T}_m$ vanish at the pole. Furthermore, to ensure that the solutions have continuous first derivatives at the pole, we also require that, for $m \neq 1$,

$$\frac{\partial \hat{v}_m}{\partial \theta} = \frac{\partial \hat{w}_m}{\partial \theta} = \frac{\partial \hat{T}_m}{\partial \theta} = 0 \quad \text{on} \quad \theta = 0,$$

For $m = 1$, the condition of continuity also requires that \hat{w}_1 and \hat{T}_1 vanish at the pole. However, no such restriction applies to the meridional velocity because the condition that $v(r, \theta, \varphi) = -v(r, \theta, \varphi + \pi)$ in the limit as $\theta \rightarrow 0$ allows for continuity in this case. However, to avoid the difficulty of computing non-zero solutions at $\theta = 0$, we only look for stability with respect to perturbations that satisfy $\hat{v}_1(r, \theta = 0) = 0$; this corresponds to perturbations that do not exhibit flow across the pole. We consider this additional boundary condition to be an additional simplifying assumption of the model. Furthermore, to reduce computational requirements we also only compute the stability with respect to perturbations that do not break the reflectional symmetry about the equator.

4. Numerical methods.

4.1. Discretization. Because it is not possible to find analytic solutions for either the steady solution or the eigenvalue problem, the solutions are approximated numerically. Second order centered finite differencing is used to discretize the spatial derivatives. We approximate the value of the unknown functions at the locations of $N \times N$ uniformly spaced grid points in the interior of the domain. The values of T on the outer boundary, on the equator, and at the pole are not determined by the boundary conditions, and must also be considered as unknowns. This leads to discretized solution vectors of size $3N^2 + 3N$. Discretization of the steady equations for u , ξ , and T leads to a system of nonlinear algebraic equations that can be solved by Newton iteration and Keller continuation (as explained in Section 4.2) to find an approximation of the steady solution.

For the numerical approximation of the eigenvalues, the linearized perturbation equations are discretized, and thus the values of the steady solution are only needed at specific locations (the grid points) and the computed approximations are used. That is, the linearization is made about the approximate solution. Thus, upon discretization the partial differential eigenvalue problem becomes a generalized matrix eigenvalue problem.

4.2. Solution techniques. We are interested in computing the steady solution for a wide range of parameter values. To do this, we implement pseudo-arclength continuation with the Keller correction condition (see e.g. [8]), and use a Newton method to solve the resulting equations. If a solution is known for a particular set of parameter values, then this method can be used effectively to follow solutions as a parameter is varied, i.e. to find a solution curve (with respect to the parameter).

Here, we know that for $\Delta T = 0$, the trivial solution satisfies the equations for u , ξ and T . Thus, for ΔT small, the trivial solution is a reasonable prediction of the solution, and Newton's method is used for the correction. In pseudo-arclength continuation, the parameter is considered as an unknown, and initial guesses of the solution are found by following the tangent, or a secant line approximation, to the solution curve. Increments are made approximately along the solution curve, and not by incrementing the parameter. The Keller condition ensures that the corrections to the initial guesses occur approximately perpendicularly to the tangent. This method is particularly useful because it is able to compute solutions along the solution curve even when there is a limit point on the curve, i.e. when the solution curve turns back on itself. In practice, the evaluation of the Jacobian is expensive, and therefore, in order to reduce the number of Jacobian evaluations, we use a quasi-Newton method in which the Jacobian is not updated on each iteration.

The generalized matrix eigenvalue problem that results from the discretization of

(3.5) is solved in Matlab using the implicitly restarted Arnoldi method [18], which is a memory-efficient iterative method for finding a specified number of the largest eigenvalues. A generalized Cayley transformation [8] is made so that the Arnoldi iteration finds the eigenvalues of interest. In particular, the generalized Cayley transformation

$$\mathbf{C}(\mathbf{L}, \mathbf{A}) = (\mathbf{L} - \alpha_1 \mathbf{A})^{-1} (\mathbf{L} - \alpha_2 \mathbf{A}) \quad (4.1)$$

maps eigenvalues λ of the generalized matrix eigenvalue problem $\lambda \mathbf{A}v = \mathbf{L}v$ to eigenvalues σ of the transformed matrix $\mathbf{C}(\mathbf{L}, \mathbf{A})$, such that the eigenvalues λ with $\text{Real}(\lambda) > (\alpha_1 + \alpha_2)/2$ are mapped to the eigenvalues σ with $|\sigma| > 1$, where α_1 and α_2 are the real parameters of the Cayley transformation. The parameters of the transformation can be chosen to improve convergence properties. The matrix $\mathbf{C}(\mathbf{L}, \mathbf{A})$ does not have to be formed explicitly, because the Arnoldi iteration only requires matrix-vector products involving $\mathbf{C}(\mathbf{L}, \mathbf{A})$ [18]. Thus, the full sparseness properties of \mathbf{L} and \mathbf{A} can be exploited, and computer memory requirements can be reduced.

5. Existence and stability results. The specific values of the parameters that are used in the computations are listed in Table 5.1. While these parameters remain fixed, we vary the gap width R (and thus $r_b \equiv r_a + R$) differential heating ΔT , and the rate of rotation Ω , and compute the azimuthal (or zonal) fluid velocity u , the stream function ξ , and temperature deviation T .

TABLE 5.1

The parameters of the spherical shell and fluid used in the computations. See Section 2 for definitions of the symbols.

r_a	10	cm
ν	$1.01e^{-2}$	cm^2/sec
κ	$1.41e^{-3}$	cm^2/sec
α	$2.06e^{-4}$	$1/^\circ \text{C}$
ρ_0	0.998	gm cm^3
T_r	20.0	$^\circ \text{C}$
g	980	cm/sec^2

For $\Delta T = 0$, there is no movement of the fluid. However, for all $\Delta T > 0$ fluid motion is induced. For small values of $\Delta T > 0$ a single convection cell develops which we call a Hadley cell. An example of such a solution for gap width $R = 3.4$ and rotation rate $\Omega = 0.01$ is plotted in Figure 5.1. In the figure, the stream function $\xi = \xi(r, \theta)$, the azimuthal (zonal) velocity $u = u(r, \theta)$, and the temperature deviation from the temperature on the inner boundary $T = T(r, \theta)$, are plotted on the unscaled domain $r_a \leq r \leq r_b$, $0 \leq \theta \leq \pi/2$. The figure represents a cross-section of the solution at an arbitrary value of the azimuthal variable φ . The solution corresponding to the full equations (2.2)–(2.4) is obtained by rotating about the polar axis and reflecting across the equator. The ‘+’ and ‘−’ indicate the contours corresponding to positive and negative values of the functions, respectively. Contours of the stream function ξ and the azimuthal velocity u that intersect the inner and outer boundaries necessarily correspond to zeros of the functions, while contours of the temperature deviation T that intersect the inner boundary correspond to zeros. The polar velocity v and the radial velocity w can be found from the stream function ξ using (3.1). In particular, the component of \mathbf{u} that lies within a meridional plane is tangential to the contours represented in Figure 5.1(a), and thus the flow tends to follow these contours. More

specifically, streamlines of the flow are restricted to lie on isosurfaces of ξ . The arrows in Figure 5.1(a) indicate the direction of the flow along the contours. In particular, in this flow, the fluid rises at the equator and falls at the pole. For this figure and all others that follow, we have taken $N = 40$.

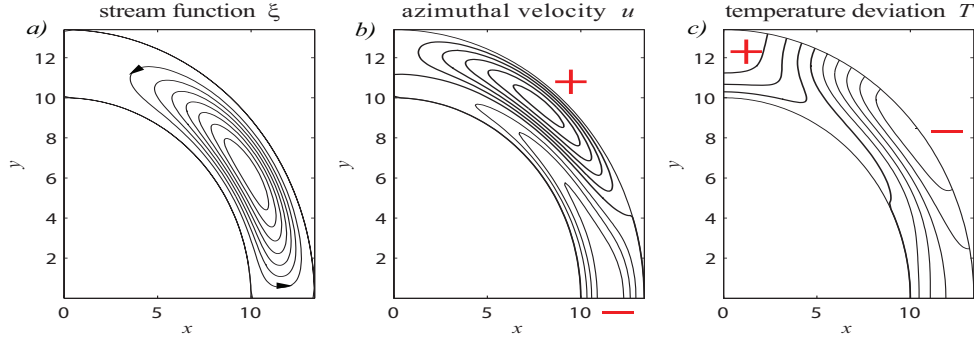


FIG. 5.1. An example of a single-cell circulation pattern observed for heating parameter $\Delta T = 0.0016$, gap width $R = 3.4$, and rotation rate $\Omega = 0.01$. (a) The stream function ξ ; the flow tends to follow the contours, (b) the azimuthal (or zonal) velocity u , and (c) the temperature deviation T from the temperature prescribed on the lower boundary.

The eigenvalues with the 10 largest real parts associated with the axisymmetric eigenfunctions, as well as those associated with the eigenfunctions for each wave number m between 1 and 8 are approximated using the techniques described in Section 3. It is found that all eigenvalues that are computed have negative real part. For the larger values of the wave number m , the eigenvalues become more negative as the wave number is increased. Thus we expect that all eigenvalues associated with all wave numbers have negative real parts, and we conclude that the circulation pattern in Figure 5.1 is a linearly stable solution of the full three-dimensional equations.

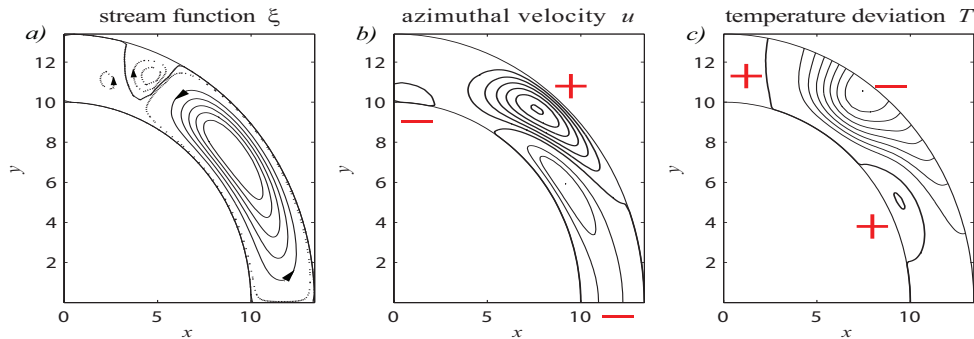


FIG. 5.2. An example of a three-cell circulation pattern observed for heating parameter $\Delta T = 0.0036$, gap width $R = 3.4$, and rotation rate $\Omega = 0.01$. (a) The stream function ξ ; the flow tends to follow the contours, (b) the azimuthal (or zonal) velocity u , and (c) the temperature deviation T from the temperature prescribed on the lower boundary. In (a), the dashed lines represent contours at $1/20$ of the interval of the solid contours.

If the heating parameter ΔT is increased further while keeping the gap width R fixed, a transition is observed. First, the flow passes through an intermediate stage, in which the stream function near the pole flattens. Then as ΔT is increased further, a

three-cell pattern develops (see Figure 5.2). The three-cell pattern resembles the zonally (azimuthally) averaged circulation pattern observed in the Earth's atmosphere, with a strong cell close to the equator (the Hadley cell), a weaker counter-rotating cell in the midlatitude (sometimes called the Ferrel cell), and finally an even weaker cell near the pole with the same direction of rotation as the Hadley cell [29]. Distinct differences between this pattern and that observed in the Earth's atmosphere is that the equatorial cell extends to higher latitude than the Hadley cell of the atmosphere, and the middle cell does not extend to the inner sphere as does the corresponding cell of the atmosphere. However, as the differential heating ΔT is increased further the middle cell does extend to the inner surface. The azimuthal velocity u is also similar to the azimuthally averaged azimuthal velocity observed in the Earth's atmosphere, except that in the atmosphere the jet stream occurs at a somewhat lower latitude, and the negative velocity near the surface does not extend as far from the equator [29]. It is found that this solution is linearly stable to all axisymmetric and non-axisymmetric perturbations considered, although stability to non-axisymmetric perturbations is lost as the differential heating is increased ΔT .

It is of particular interest that, although there is clearly a transition in the flow pattern as ΔT is increased, there is no point at which the solution is neutrally stable, i.e. no eigenvalue crosses the imaginary axis. This is not entirely unexpected. Other studies in which flow transitions in systems with a lack of symmetry were investigated have revealed such behaviour; for example see [7, 23, 15, 30, 27]. Although such transitions have been observed in the absence of a corresponding nearby bifurcation (e.g. [7, 23]), they may be induced by a broken pitchfork bifurcation or a perturbed hysteresis bifurcation (see below). Therefore, we search for such a mechanism.

Although our full system has $SO(2) \times \mathbb{Z}_2$ symmetry, we are looking for solutions that preserve this symmetry, so we have used the symmetry to simplify the equations for u , ξ and T . The simplified equations possess none of these symmetries. The symmetries of a system determine the types of bifurcation that are likely to occur, i.e. which types are generic for the system. For equations with no symmetry, saddle-node and Hopf bifurcations are generic, and are expected to be observed if a real eigenvalue crosses through zero or a complex pair of eigenvalues crosses the imaginary axis, respectively, as a single parameter is varied.

The presence of a saddle-node bifurcation in itself can not explain the observed transition, which occurs without a zero eigenvalue. However, such a transition may occur near an organizing center or bifurcation of codimension 2. This implies that it will be necessary to vary a second parameter to find it. The types of codimension 2 bifurcation points that could occur generically in a system like ours are the broken pitchfork bifurcation [10, 15, 30] and the hysteresis (or cusp) bifurcation [27] as described above and in [10, 16].

In order to clarify the origin of the observed transition, it is useful to explore the solutions at larger gap width and rate of rotation. If the gap width is increased to $R = 12$ and the rotation rate to $\Omega = 0.1$, then, when the heating ΔT is small enough, the linearly stable one-cell pattern is maintained, with a slight distortion of the stream function near the outer boundary, and an increase in the retrograde velocity near the equator. An example is plotted in Figure 5.3. As the heating parameter ΔT is increased, there is a transition to a two-cell pattern (Figure 5.4), and again this transition occurs without an eigenvalue corresponding to an axisymmetric eigenfunction crossing the imaginary axis.

It is observed that as the gap width R and the rotation rate Ω are increased,

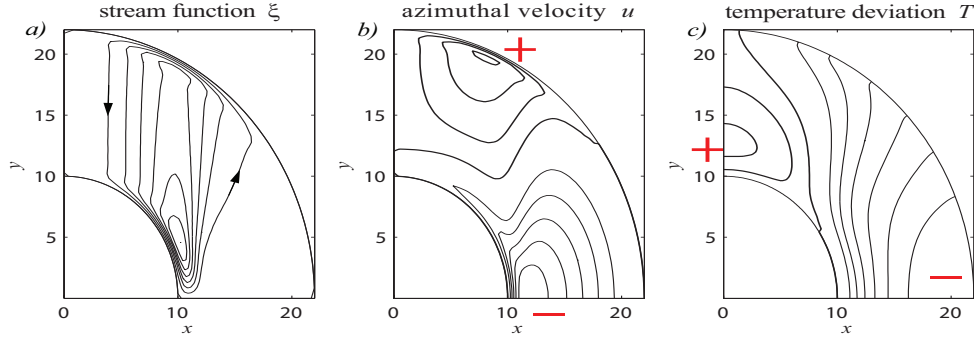


FIG. 5.3. An example of a single-cell circulation pattern observed for heating parameter $\Delta T = 0.014$, gap width $R = 12$, and rotation rate $\Omega = 0.1$. (a) The stream function ξ ; the flow tends to follow the contours, (b) the azimuthal (or zonal) velocity u , and (c) the temperature deviation T from the temperature prescribed on the lower boundary.

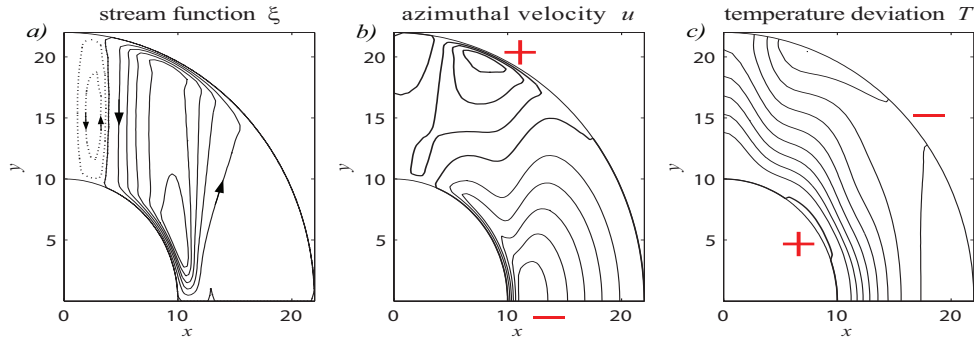


FIG. 5.4. An example of a two-cell circulation pattern observed for heating parameter $\Delta T = 0.016$, gap width $R = 12$, and rotation rate $\Omega = 0.1$. (a) The stream function ξ ; the flow tends to follow the contours, (b) the azimuthal (or zonal) velocity u , and (c) the temperature deviation T from the temperature prescribed on the lower boundary. In (a), the dashed lines represent contours at $1/5$ of the value of the solid contours.

the steady solutions become less stable to non-axisymmetric perturbations. As a result, although this two-cell pattern is stable to axisymmetric perturbations, it is linearly unstable to non-axisymmetric perturbations. The loss of stability to the non-axisymmetric perturbations occurs as a Hopf bifurcation, and thus the bifurcating solution is expected to be a rotating wave with azimuthal wave number m . This implies that this two-cell solution will not be physically observable directly. However, because the loss of stability occurs near the one-cell to two-cell transition, it is possible that the rotating wave will inherit the θ and r dependence of the two-cell solution, i.e. an azimuthal average of the rotating wave will have a two-cell structure. We do not show this here, as it is secondary to our purpose for presenting this example. Regardless of the stability with respect to non-axisymmetric perturbations, the two-cell pattern is a linearly stable solution of the axisymmetric equations, and forms in qualitatively the same manner as the transition that is observed at lower R and Ω (see below for further discussion). Thus, an investigation of the transition to this flow, in the axisymmetric equations, will provide a mechanism for the transition. Below we consider only solutions and stability with respect to the axisymmetric equations.

As mentioned above, the transition at $R = 12$ and $\Omega = 0.1$ occurs without an eigenvalue corresponding to an axisymmetric eigenfunction crossing the imaginary axis. Because the eigenvalue with largest real part is real, this implies that there is no parameter value at which there is a zero eigenvalue. In Figure 5.5, we plot the real value of the (axisymmetric) eigenvalue with largest real part as a function of the heating parameter ΔT , and we plot a “bifurcation diagram” that indicates how the solutions change as ΔT changes, where the vertical axis is the L^2 -norm of the stream function ξ . In the figure it can be seen that as the heating parameter ΔT increases, the value of the eigenvalue increases until it reaches a maximum that is negative, at which point it begins to decrease without ever reaching zero. Heuristically, it is observed that the development of the two-cell pattern begins to occur near this maximum.

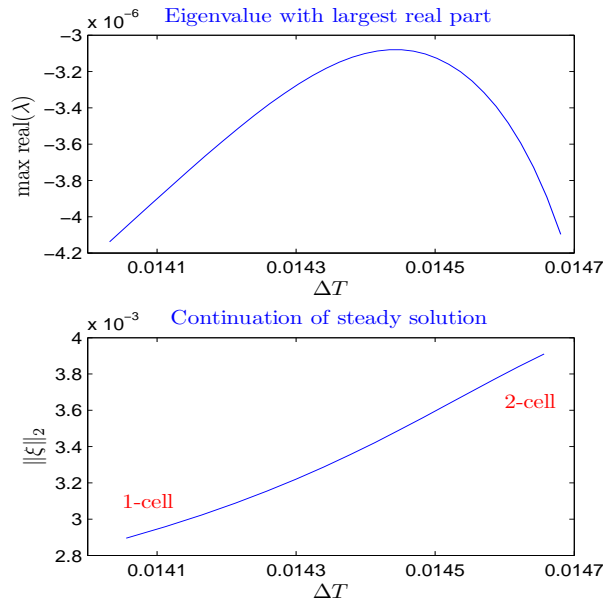


FIG. 5.5. Results for $R = 12$, $\Omega = 0.1$. (top) Real part of eigenvalue with largest real part versus ΔT , and (bottom) Bifurcation diagram in ΔT ; vertical axis represents the L^2 -norm of the stream function ξ .

If the gap width is increased to $R = 16.2$, then for small values of ΔT a linearly stable one-cell pattern is again observed. See Figure 5.6. A gap width of $R = 16.2$ corresponds to an aspect ratio $\eta = R/r_a = 1.35$. Although we are not necessarily interested in flows at large aspect ratio, they will help to explain the transition that is observed for smaller gap width.

As we increase the differential heating ΔT , again we see a transition from the one-cell to a two-cell pattern, shown in Figure 5.7. However, in this case, a real eigenvalue does cross the imaginary axis. In Figure 5.8, we plot both the real part of the eigenvalue with largest real part as a function of ΔT , and the corresponding bifurcation diagram. The crossing of the imaginary axis by a real eigenvalue corresponds to a saddle-node bifurcation, also referred to as a limit point or fold. As the solution curve is followed past the bifurcation point, the solution becomes linearly unstable, and the value of ΔT begins to decrease. For a short interval, the real eigenvalue increases until it reaches a maximum, after which it begins to decrease. Subsequently, it again

crosses the imaginary axis, and a second saddle-node bifurcation is observed. As we follow the curve past this point, the solution returns to being linearly stable, and ΔT once again begins to increase. This pair of saddle-node bifurcations results in an ‘S’ shaped bifurcation diagram. As we follow the solution curve, from the lower part of the ‘S’ to the upper part of the ‘S’, the real part of the eigenvalue with largest real part traces out the loop seen in Figure 5.8. This form of solution curve results in a classical mechanism for hysteresis, as seen in the hysteresis loop shown in Figure 1.1.

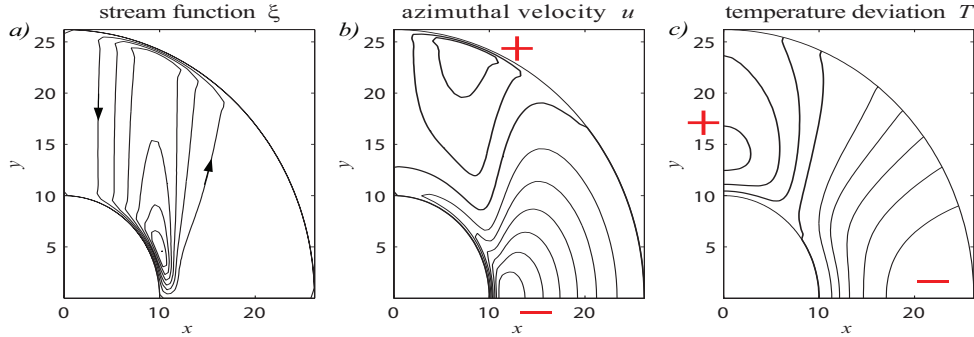


FIG. 5.6. An example of a single-cell circulation pattern observed for heating parameter $\Delta T = 0.013$, gap width $R = 16.2$, and rotation rate $\Omega = 0.1$. (a) The stream function ξ ; the flow tends to follow the contours, (b) the azimuthal (or zonal) velocity u , and (c) the temperature deviation T from the temperature prescribed on the lower boundary.

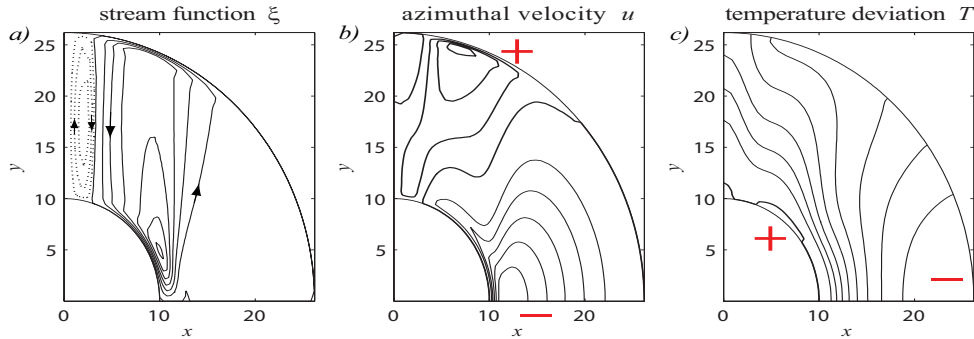


FIG. 5.7. An example of a two-cell circulation pattern observed for heating parameter $\Delta T = 0.015$, gap width $R = 16.2$, and rotation rate $\Omega = 0.1$. (a) The stream function ξ ; the flow tends to follow the contours, (b) the azimuthal (or zonal) velocity u , and (c) the temperature deviation T from the temperature prescribed on the lower boundary. In (a), the dashed lines represent contours at $1/5$ of the value of the solid contours.

6. Hysteresis bifurcation. The behaviour observed in Figures 5.5 and 5.8 is indicative of a hysteresis (or cusp) bifurcation point. The typical behaviour of a nonlinear system near a hysteresis point is as shown in Figure 1.1. It can be expected that at some critical value of the gap width $R = R_c$, a one-dimensional bifurcation diagram in ΔT will have a single vertical tangent, with slopes on either side being positive. For values of $R < R_c$, we expect no bifurcations as ΔT is increased (as in Figure 5.5), while for $R > R_c$ we expect a pair of saddle-node bifurcations (as in Figure 5.8). This behaviour can be seen in Figure 1.1, where these different one-

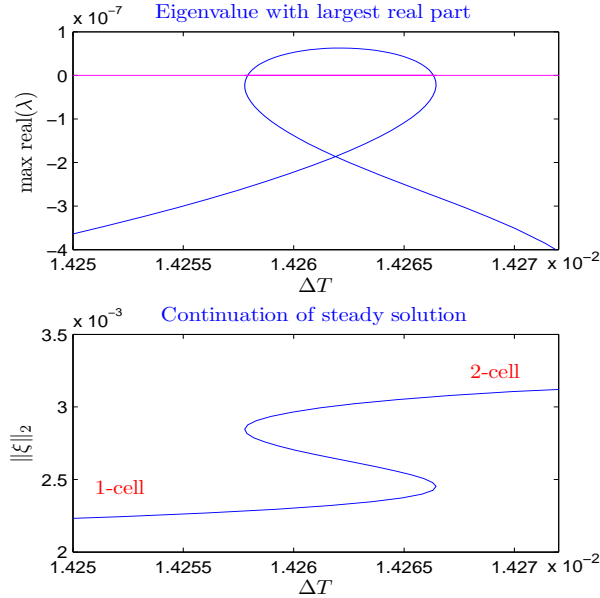


FIG. 5.8. Results for $R = 16.2$. (top) Real part of eigenvalue with largest real part versus ΔT , and (bottom) Bifurcation diagram in ΔT ; vertical axis represents the L^2 -norm of the stream function ξ

dimensional bifurcation diagrams in ΔT may be obtained as slices through M , taken with different values of constant R . Mathematically, a hysteresis or cusp bifurcation point is determined by the following three conditions [16]:

1. There exists a steady solution.
2. There is a simple zero eigenvalue of the linearization of the equations about the steady solution.
3. The coefficient of the second order term of the normal form equations on the centre manifold vanishes.

Therefore, in order to demonstrate that the observed behaviour is indeed generated by a hysteresis bifurcation, it is necessary to show that each of the above three conditions is satisfied. Although it may seem that this would be a daunting task, in fact these conditions can be verified by an explicit calculation that can be performed numerically as follows, see [8, 16]. To elucidate these conditions and the means that we use to compute the hysteresis point, we write the equations for ξ , u , and T in the abstract form:

$$\dot{U} = LU + N(U, U), \quad (6.1)$$

where

$$U = \begin{pmatrix} \xi \\ u \\ T \end{pmatrix}$$

is the dependent variable, L is the linear operator such that LU is the linear part of the equations, $N(U, U)$ is the nonlinear part of the equations, and the dot represents differentiation with respect to time. Note that the nonlinear part N has only quadratic

terms (from the Navier-Stokes equation), and thus we may write it in the bilinear form $N(U, U)$.

Assume that for some critical values of the parameters $(\Delta T, R) = (\Delta T_c, R_c)$, there is a steady solution U_0 of (6.1), i.e., U_0 satisfies

$$LU_0 + N(U_0, U_0) = 0. \quad (6.2)$$

Assume also that at $(\Delta T, R) = (\Delta T_c, R_c)$ the linearization L_0 about the steady solution U_0 has a simple zero eigenvalue $\lambda_0 = 0$ while all other eigenvalues have negative real part, where L_0 is given by

$$L_0 V = LV + N(V, U_0) + N(U_0, V). \quad (6.3)$$

That is, we have

$$L_0 \Psi = 0, \quad (6.4)$$

where Ψ is the eigenfunction corresponding to the zero eigenvalue.

Under certain conditions on L_0 , the dependent variable U can be written in the form

$$U = w\Psi + \Phi, \quad (6.5)$$

where $w \in \mathbb{R}$ and thus $w\Psi \in \text{span}\{\Psi\}$, and $\Phi \in E_s$. Here E_s is called the stable subspace, and is the space spanned by all eigenfunctions corresponding to eigenvalues with negative real part.

If we write U as in (6.5) then under certain technical conditions, a centre manifold and normal form reduction can be performed on (6.1) to obtain the equation on the centre manifold in normal form

$$\dot{w} = \beta_1 + \beta_2 w + aw^2 + cw^3 + O(w^4), \quad (6.6)$$

where a and c are coefficients of the normal form, and β_1 and β_2 are unfolding parameters that are in general functions of the parameters ΔT and R . It can be shown that if $c \neq 0$, then neglecting the terms of $O(w^4)$ do not change the qualitative features of the solutions.

The centre manifold and normal form theories state that for $(\Delta T, R)$ near $(\Delta T_c, R_c)$ and when the solutions are in some sense small, then the dynamics of (6.1) can be deduced from (6.6). In particular, solutions of (6.6) are in one-to-one correspondence with those of (6.1).

Formulas for the coefficients of the normal form equation can be derived by performing a centre manifold and normal form reduction in the general case [8, 16]. In particular, the coefficient of the second order term is given by

$$a = 1/2 \langle \Psi^*, N(\Psi, \Psi) \rangle, \quad (6.7)$$

where Ψ is the eigenfunction corresponding to λ_0 , Ψ^* is the corresponding adjoint eigenfunction corresponding to λ_0 , and

$$\langle U, V \rangle = \iint U \cdot V \, d\mathbf{r} \quad (6.8)$$

is the inner product on the domain.

For $a = 0$, a hysteresis bifurcation occurs when $\beta_1 = \beta_2 = 0$. For $\beta_2/c > 0$, there is a single solution to (6.6) for all β_1 . For $\beta_2/c < 0$, there is a region in the two-dimensional parameter space (β_1, β_2) in which there are three solutions. The borders of this region are given asymptotically by the two curves

$$\beta_1 = \pm \frac{2}{3} \sqrt{\frac{-\beta_2}{c}} \beta_2. \quad (6.9)$$

As β_2 approaches zero, these two curves approach each other and meet in a cusp at $\beta_1 = \beta_2 = 0$. This is the origin of the name ‘‘cusp bifurcation’’.

In order to show that a hysteresis or cusp bifurcation occurs in the model, we need to show that the three aforementioned conditions are satisfied. That is, we must find parameter values $(\Delta T, R) = (\Delta T_c, R_c)$, such that the following three equations are satisfied

$$LU_0 + N(U_0, U_0) = 0, \quad (6.10)$$

$$L_0V = 0, \quad \langle V, V \rangle = 1, \quad (6.11)$$

$$a = 1/2 \langle \Psi^*, N(\Psi, \Psi) \rangle = 0, \quad (6.12)$$

where L_0 is given by (6.3).

These equations have the unfortunate property that for some values of $\Delta T \neq \Delta T_c$, $R \neq R_c$, L_0 will not be singular, and thus (6.11) will not have a solution for any V . Therefore, it will be convenient to use the following defining system [8]

$$LU_0 + N(U_0, U_0) = 0, \quad (6.13)$$

$$g = 0, \quad (6.14)$$

$$g' = 0, \quad (6.15)$$

where g and g' are scalars given by

$$L_0V + gB = 0, \quad \langle C, V \rangle = 1, \quad (6.16)$$

$$L_0V' + g'B = -N(V, V), \quad \langle C, V' \rangle = 0, \quad (6.17)$$

and where B is not in the range of L_0 , and C is not in the range of the adjoint operator L_0^* , which is defined by

$$\langle L_0U, V \rangle = \langle U, L_0^*V \rangle,$$

for all U and V .

Each of the three equations (6.13) – (6.15) corresponds to one of the hysteresis point defining conditions. Specifically, U_0 is a steady solution of (6.1) when the first equation (6.13) is satisfied. If we set $g = 0$ in (6.16) and there is a solution, then L_0 has a zero eigenvalue with corresponding eigenfunction V . Thus, the second hysteresis condition is satisfied when the second equation (6.14) is satisfied. In this case, when L_0 is not singular then there will still be a solution of (6.16), namely one for which $g \neq 0$. This is assured by choosing B not in the range of L_0 . If we set $g' = 0$ in (6.17), and there is a solution, then we have that $N(V, V)$ must be in the range of L_0 . If we also have $g = 0$, then from above we have that V is the eigenfunction of L_0 with zero eigenvalue, i.e. $V = \Psi$. Thus, if $N(V, V)$ is in the range of L_0 then,

by the ‘‘Fredholm alternative’’ property of the adjoint, $N(V, V)$ must be orthogonal to the eigenfunction of L_0^* corresponding to the zero eigenvalue, i.e. we must have $\langle \Psi^*, N(\Psi, \Psi) \rangle = 0$, and thus the second-order coefficient of the normal form vanishes. When L_0 is nonsingular, (6.17) has a solution regardless of g' . However, there is also the possibility that close to the cusp there are parameter values such that L_0 is singular, while $N(V, V)$ is not in the range of L_0 ; this occurs at the saddle-node bifurcations. Thus, there will be no solution of (6.17) for $g' = 0$. However, because B is not in the range of L_0 , we are assured a solution with $g' \neq 0$.

In order to make the equations linear in V and V' , we can choose the normalization conditions as shown. Solutions are assured when C is chosen to be not in the range of the adjoint operator L_0^* . In practice, because the kernel of L_0 is only one dimensional, it is easy to choose B and C with the required properties.

It can be proved that when the system (6.13) – (6.15) has a solution, then not only is the non-degeneracy condition for a cusp bifurcation satisfied, but also the transversality condition [8]. Thus, we are assured that we have found a cusp bifurcation.

Upon discretization of (6.13) – (6.15) and (6.16) – (6.17) on an $N \times N$ grid, we obtain a system of nonlinear algebraic equations. For various values of N , we find that there are critical parameter values $(\Delta T, R) = (\Delta T_c, R_c)$ such that there is a U_0 , g and g' that satisfy the discretized system. Results are listed in Table 6.1. Although for small N it appears that we are not in the asymptotic range, the results for higher value of N provide evidence of convergence. The large variation in R between the results at $N = 40$ and $N = 80$ is possibly caused by the nonlinear dependence of the equations on R ; see (2.9) – (2.13). In particular, for large R , we expect that a large change in R is required to produce even a small change in behaviour of the solutions. This could also be an indication that the boundary layers are not sufficiently resolved at low resolution to put us in the asymptotic range of the convergence. Regardless, the results provide evidence that a hysteresis bifurcation does in fact exist in the model with cusp point $(\Delta T_c, R_c) \approx (0.017, 28)$, and thus the lower resolution captures the correct qualitative behaviour.

TABLE 6.1

Critical parameter values at which the hysteresis bifurcation occurs, for various values of N . The results provide evidence of convergence.

N	ΔT	R
40	0.0143	16.0
80	0.0155	24.2
120	0.0163	27.8
160	0.0165	28.0

There is strong evidence that the transition from the one-cell to the two-cell pattern, that is observed at gap width $R = 12$ as the differential heating ΔT is increased, is associated with this cusp bifurcation. We also postulate that the transition from the one-cell to the three-cell pattern, that is observed at gap width $R = 3.4$ as the differential heating ΔT is increased, is not only the same mechanism, but is associated with the same bifurcation. This is evident if we consider the transition from the one-cell pattern for a sequence of gap widths R and rotation rates Ω that decrease from $R = 12$, $\Omega = 0.1$ to $R = 3.4$, $\Omega = 0.01$. For all transitions in this sequence, regardless of whether the transition results in a two-cell or three-cell pattern, the eigenvalue with largest real part behaves in the same manner (as shown in Figure 5.5) with only small

quantitative changes. Furthermore, in all cases, the stream function component of the eigenfunctions corresponding to the eigenvalue with largest real part has a two-cell structure. The azimuthal velocity component of the eigenfunctions also shows little variation. There is nothing to indicate that there is another bifurcation that is taking place. That is, all solutions discussed above lie on a single solution manifold that is folded at the cusp point; see the manifold M in Figure 1.1. In [27], such a manifold is shown to connect qualitatively different solutions in a model of rotating convection in a cylinder with centrifugal buoyancy.

Furthermore, there is a smooth variation of the qualitative behaviour as R is varied. For large R , the transition from one-cell to two-cell begins with a flattening of the stream function ξ near the pole, corresponding to a decrease in fluid velocity in this region, and is followed by the formation of the counter-rotating cell near the pole. The new cell is first observed as a small cell adjacent to the pole, and grows as the differential heating ΔT is increased. Changes in the rotation rate Ω affect the stability of the solution to non-axisymmetric perturbations, but do not affect the qualitative features of the transition, and therefore, here, we refer only to changes in gap width R . If R is decreased, the flattening becomes more pronounced before the second cell is observed. When the cell is observed, it grows more quickly with ΔT than when the gap width is larger. If the differential heating is increased sufficiently, a transition from the two-cell pattern to a three-cell pattern is observed. For yet smaller gap width, (e.g. $R = 3.4$), again the transition begins with a flattening. However, in this case, the second cell does not first appear adjacent to the pole, but peeks out a small distance from the pole. This transitional stage is not in essence a two-cell pattern, because between the new cell and the pole there is a very weak (almost quiescent) region in which the fluid rotates in the same sense as the large cell near the equator.

The development of the two-cell pattern is easily explained in terms of the lowest order dynamics of the cusp bifurcation. To lowest order, the solution U to the perturbation equations will be given by $w\Psi$, where $w \in \mathbb{R}$, and Ψ is the eigenfunction corresponding to the eigenvalue with largest real part, see (6.5). Thus, to first order, the solution to the axisymmetric equations will be $w\Psi$ plus the solution about which we have linearized, i.e., the one-cell solution. Thus, because the stream function component of the eigenfunction Ψ has a two-cell structure, we expect that, to lowest order, the solution will also develop a two-cell structure. The development of the three-cell pattern in this context is not as easily explained. However, it may be possible that insight could be gained from a higher order computation.

We have already pointed out that the variation of the rotation rate Ω has relatively smaller qualitative effect on the solutions of the axisymmetric equations. Indeed, a cusp is observed if the rotation is held fixed at $\Omega = 0.01$, and only the gap width R is increased. We choose not to present this example because, in this case, an additional saddle-node bifurcation occurs at values of the differential heating slightly larger than where the cusp is observed. As the rotation rate is increased, this bifurcation moves further away from the cusp, and thus the example for $\Omega = 0.1$ more clearly indicates the origin of the observed transitions.

7. Discussion and Conclusions. This work has shown that a Boussinesq fluid in a rotating spherical shell, differentially heated on its inner surface, can exhibit a variety of stable rotationally symmetric flow patterns. Distinctive features of these flow patterns include a Hadley cell with a flow pattern much like the Hadley cells of the Earth, and a high azimuthal velocity jet stream located at high altitudes and mid-latitudes, much like the jet stream in each hemisphere of the Earth. For small

values of the differential heating parameter $\Delta T > 0$, the Hadley cell exists and extends from equator to pole. For larger values of ΔT , first one then two or more additional convection cells may form between the Hadley cell and the pole in the mid and polar latitudes. The first cell to form after the Hadley cell exhibits counter-rotating flow (westerly winds near the inner surface) and the third cell has Hadley-like rotation (easterly winds near the polar surface). The observed transitions are distinctly related to the spherical geometry of the system. This is evident because in all models of differentially heated fluids in domains with cylindrical geometry, such transition that do not break the rotational symmetry only occur at very high differential heating.

The features of the transitions are not affected by moderate changes in the rate of rotation Ω , although the solutions become less stable to non-axisymmetric perturbations as Ω is increased. However, changes in the gap width R can induce significant changes. Mathematical analysis of the axisymmetric model demonstrates that it possesses a codimension two hysteresis (or cusp) bifurcation for a critical choice of the parameters $(R, \Delta T) = (R_c, \Delta T_c)$. In a neighborhood of this hysteresis point, for larger R , there exists a region of bistability in which two different states of the system are both linearly stable solutions of the axisymmetric equations. These two stable states are separated by a third unstable state. For such R (fixed), there exists an interval of values of ΔT exhibiting a hysteresis loop as illustrated in Figure 1.1. At each end of this interval, a small change in ΔT can cause a transition in the state of the system, to a qualitatively different flow pattern, e.g. one with a different number of convection cells.

The results of this paper lead to more questions than answers, and will form the basis of much future work. In the model, changes in the Hadley cell have no influence on the temperature difference parameter ΔT . This is not the case in a real planetary system, where convection cells are known to act as “thermal conveyor belts”. In the case of small ΔT and a large Hadley cell extending from equator to pole, this conveyor belt would have the effect of warming the polar region and cooling the equatorial region, thus *reducing* the temperature difference ΔT . This can be seen in the temperature deviation plots of Figures 2 and 4, in which the gradient of the temperature deviation is essentially opposite to the imposed differential heating. Therefore, the thermal conveyor belt function of a large Hadley cell enhances its persistence. On the other hand, if ΔT increases (for some other reason) to a value where the single Hadley cell is replaced by multiple cells, this would curtail the thermal conveyor belt acting from equator to pole. As a result, the polar regions would cool relative to the equatorial regions and ΔT would increase, pushing the system further to the right along the bifurcation curve. We conjecture that this feedback mechanism, from the convection cell flow back to the temperature difference ΔT , is present in real planetary atmospheres and implies a modification of the predictions of our model. The effect is most easily stated with reference to Figure 1.1: the interval of bistability in ΔT would lengthen and the cusp point would move to smaller values of R . In other words, the net effect of this thermal feedback would be to increase both the likelihood and the amplitude of the hysteresis behaviour demonstrated in the model.

In addition, the model should be reconsidered to take into account the fact that the atmosphere of the earth is a strongly stratified compressible fluid, with properties very different from water. The vertical motion of a strongly stratified fluid is inhibited, thus causing an elongation (in θ) of the cells. The cells in a Boussinesq fluid typically have an aspect ratio close to 1, which implies that R must be rather large in order to see only 3 cells. In a strongly stratified fluid, a much smaller R (for a similar ΔT)

would be sufficient to see a similar number of cells. Therefore, we predict that the phenomena exhibited in this model could exist in the atmosphere of a planet such as the earth, but for much smaller aspect ratios R/r_a . Thus, both the thermal feedback and the stratified fluid properties of real atmospheres, which have been neglected in this simple model, can be expected to amplify rather than inhibit the hysteresis mechanism demonstrated for the model.

In further work the model could be extended to physical dimensions on the scale of a planet such as the Earth. Another future goal is an analysis of the non-axisymmetric bifurcations that would lead to rotating waves as well as analyses of spherical shell models that break the north-south reflectional symmetry or satisfy different boundary conditions.

Acknowledgments. The authors would like to thank Wayne Nagata, Martin Golubitsky and Laurette Tuckerman for helpful discussions, and would like to thank the referees for their helpful comments.

REFERENCES

- [1] D. J. ACHESON, *Elementary Fluid Dynamics*. Oxford Applied Mathematics and Computing Science Series, Clarendon Press, Oxford, UK, 1990.
- [2] C. D. ANDERECK AND F. HAYOT, *Ordered and Turbulent Patterns in Taylor-Couette Flow*. NATO ASI Series Physics 297, Plenum, New York, 1992.
- [3] P. BELTRAME, V. TRAVNIKOV, M. GELLERT, AND C. EGBERS, *GEOFLOW: simulation of convection in a spherical shell under central force field*, *Nonlin. Processes Geophys.*, 13 (2006), pp. 413–423.
- [4] S. CHANDRASEKHAR, *Hydrodynamic and Hydromagnetic Stability*. Dover Publications, New York, 1981. (first published 1961, Oxford University Press).
- [5] P. CHOSSAT, *Bifurcation and stability of convective flows in a rotating or not rotating spherical shell*, *SIAM J. Appl. Math.*, 37 (1979), pp. 624–647.
- [6] P. CHOSSAT AND G. IOOSS, *The Couette-Taylor Problem*. Springer-Verlag, New York (1994).
- [7] M. P. ESCUDIER, *Observations of the flow produced in a cylindrical container by a rotating endwall*, *Exper. in Fluids*, 2 (1984), pp. 189–196.
- [8] W. J. F. GOVAERTS, *Numerical Methods for Bifurcations of Dynamical Equilibria*. SIAM, Philadelphia, 2000.
- [9] M. GOLUBITSKY AND W. F. LANGFORD, *Pattern formation and bistability in flows between counterrotating cylinders*, *Physica D*, 32 (1988), pp. 362–392.
- [10] M. GOLUBITSKY AND D. G. SCHAEFFER, *Singularities and Groups in Bifurcation Theory*, *Appl. Math. Sci.* 51, Springer-Verlag, New York, 1985.
- [11] J. E. HART, G. A. GLATZMAIER, AND J. TOOMRE, *Space-laboratory and numerical simulations of thermal convection in a rotating hemispherical shell with radial gravity*, *J. Fluid Mech.*, 173 (1986), pp. 519–544.
- [12] R. HIDE AND P. J. MASON, *Sloping convection in a rotating fluid*, *Adv. Geophys.*, 24 (1975), pp. 47–100.
- [13] P. HIGNETT, A. A. WHITE, R. D. CARTER, W. D. N. JACKSON, AND R. M. SMALL, *A comparison of laboratory measurements and numerical simulations of baroclinic wave flows in a rotating cylindrical annulus*, *Quart. J. Roy. Meteorol. Soc.*, 111 (1985), pp. 131–154.
- [14] R. HOLLERBACH, *Instabilities of the Stewartson layer Part 1. The dependence on the sign of R_o* , *J. Fluid Mech.*, 492 (2003), pp. 289–302.
- [15] A. JUEL, A. G. DARBYSHIRE, AND T. MULLIN, *The effect of noise on pitchfork and Hopf bifurcations*, *Proc. Roy. Soc. Lond. A*, 453 (1997), pp. 2627–2647.
- [16] Y.A. KUZNETSOV, *Elements of Applied Bifurcation Theory*. Third Edition. Springer-Verlag, New York, 2004.
- [17] W. F. LANGFORD, R. TAGG, E. J. KOSTELICH, H. L. SWINNEY, AND M. GOLUBITSKY, *Primary instabilities and criticality in flow between counter-rotating cylinders*, *Phys. Fluids*, 31 (1988), pp. 776–785.
- [18] R. LEHOUCQ, D. C. SORENSEN, AND C. YANG, *ARPACK Users' Guide: Solution of Large-Scale Eigenvalue Problems with Implicitly Restarted Arnoldi Methods*. SIAM, Philadelphia, 1998.

- [19] V. LESUEUR, A. ABOUELAININE, A. MANGENEY, AND P. DROSSART, *Geostrophic motions of a Boussinesq fluid in a thick rotating spherical shell*, Geophys. Astrophys. Fluid Dyn., 91 (1999), pp. 1–43.
- [20] G. M. LEWIS AND W. NAGATA, *Linear stability analysis for the differentially heated rotating annulus*, Geophys. and Astrophys. Fluid Dyn., 98 (2004), pp. 129–152.
- [21] G. M. LEWIS AND W. NAGATA, *Double Hopf bifurcations in the differentially heated rotating annulus*, SIAM J. Appl. Math., 63 (2003), pp. 1029–1055.
- [22] L. LI, P. ZHANG, X. LIAO, AND K. ZHANG, *Multiplicity of nonlinear thermal convection in a spherical shell*, Phys. Review E, 71 (2005)
- [23] J. M. LOPEZ, *Axisymmetric vortex breakdown Part 1. Confined swirling flow*, J. Fluid. Mech., 221 (1990), pp. 533–552.
- [24] E. N. LORENZ, *The Nature and Theory of the General Circulation of the Atmosphere*. World Meteorological Society, 1967.
- [25] P. S. MARCUS AND L. S. TUCKERMAN, *Simulation of flow between concentric rotating spheres. Part 1. Steady states*, J. Fluid Mech., 185 (1987), pp. 1–30.
- [26] P. S. MARCUS AND L. S. TUCKERMAN, *Simulation of flow between concentric rotating spheres. Part 2. Transitions*, J. Fluid Mech., 185 (1987), pp. 31–65.
- [27] F. MARQUES, I. MERCADER, O. BATISTE, AND J. M. LOPEZ, *Centrifugal effects in rotating convection: axisymmetric states and three-dimensional instabilities*, J. Fluid. Mech., 580 (2007), pp. 303–318.
- [28] S. W. MORRIS, J. R. DE BRUYN, AND A. D. MAY, *Patterns at the onset of electroconvection in freely suspended smectic films*, J. Stat. Phys. 64 (1991), pp. 1025–1043.
- [29] J. P. PEIXOTO AND A. H. OORT, *Physics of Climate*. American Institute of Physics, New York, 1992.
- [30] A. M. RUCKLIDGE AND A. R. CHAMPNEYS, *Boundary effects and the onset of Taylor vortices*, Physica D, 191 (2004), pp. 282–296.
- [31] G. P. WILLIAMS, *Baroclinic annulus waves*, J. Fluid Mech., 49 (1971), pp. 417–449.
- [32] T. YANAGISAWA AND Y. YAMAGISHI, *Rayley-Bénard convection in a spherical shell with infinite Prandtl number at high Rayleigh number*, J. Earth Sim., 4 (2005), pp. 11–17.